Naval Research Laboratory

Washington, DC 20375-5320

NRL/MR/5675--19-9854

Development and Characterization of a Fiber Optic Thermal Insulator (FOTI)

Gary A. Miller

Optical Techniques Branch
Optical Sciences Division

April 1, 2019

REPORT DOCUMENTATION PAGE

Form Approved
OMB No. 0704-0188

1. REPORT DATE *(DD-MM-YYYY)* 01-04-2019	**2. REPORT TYPE** Memorandum Report	**3. DATES COVERED** *(From - To)*
4. TITLE AND SUBTITLE Development and Characterization of a Fiber Optic Thermal Insulator (FOTI)		**5a. CONTRACT NUMBER** **5b. GRANT NUMBER** **5c. PROGRAM ELEMENT NUMBER** 62747N
6. AUTHOR(S) Gary A. Miller		**5d. PROJECT NUMBER** UW-747-021 **5e. TASK NUMBER** T051-16 **5f. WORK UNIT NUMBER** 6A36
7. PERFORMING ORGANIZATION NAME(S) AND ADDRESS(ES) Naval Research Laboratory 4555 Overlook Avenue, SW Washington, DC 20375-5320		**8. PERFORMING ORGANIZATION REPORT NUMBER** NRL/MR/5675--19-9854
9. SPONSORING / MONITORING AGENCY NAME(S) AND ADDRESS(ES) Office of Naval Research One Liberty Center 875 N Randolf Street, Suite 1425 Arlington, VA 22203-1995		**10. SPONSOR / MONITOR'S ACRONYM(S)** ONR **11. SPONSOR / MONITOR'S REPORT NUMBER(S)**

12. DISTRIBUTION / AVAILABILITY STATEMENT

DISTRIBUTION STATEMENT A: Approved for public release; distribution is unlimited.

13. SUPPLEMENTARY NOTES

14. ABSTRACT

To reduce the effect that transient temperature fluctuations had on gratings, utilization of passive temperature control via insulation was investigated. For this, a novel packaging technique involving evacuated capsules was developed. In addition to determining the required vacuum pressure needed to insulate the gratings, numerous devices were fabricated and their performance was measured. In one design, the insulator showed a 30 dB improvement in limiting temperature fluctuations and a time constant 5000 times greater than bare fiber.

15. SUBJECT TERMS

Fiber Bragg Grating, Athermalization Vacuum Insulation
Vacuum Pressure Temperature Control

16. SECURITY CLASSIFICATION OF:			**17. LIMITATION OF ABSTRACT**	**18. NUMBER OF PAGES**	**19a. NAME OF RESPONSIBLE PERSON** Gary A. Miller
a. REPORT Unclassified Unlimited	**b. ABSTRACT** Unclassified Unlimited	**c. THIS PAGE** Unclassified Unlimited	Unclassified Unlimited	16	**19b. TELEPHONE NUMBER** *(include area code)* (202) 767-9510

Standard Form 298 (Rev. 8-98)
Prescribed by ANSI Std. Z39.18

This page intentionally left blank.

CONTENTS

This page intentionally left blank.

DEVELOPMENT AND CHARACTERIZATION OF A FIBER OPTIC THERMAL INSULATOR (FOTI)

1. INTRODUCTION

Many fiber optic components such as in-fiber gratings are highly susceptible to temperature variations while in operation. The properties of these components can change dramatically with temperature potentially causing signal fading or dropout, an increase in noise, or intensity variations in a system that responds to these properties. Owning to their small size, unpackaged fiber optic components have thermal time constants on the order of 10's of milliseconds. Components subjected to thermal fluctuations slower than this time constant will respond to this, potentially affecting their performance. This is not only detrimental for low frequency or DC measurements but also undesirable for high frequency measurements where signal fading might be an issue. Example scenarios where this might cause deleterious effects are when the component is used for reference signals, optical filtering, channel filters or blocks, and wavelength locking. Temperature fluctuations can also be problematic for fiber lasers that rely on in-fiber gratings and splice joints between dissimilar materials or structures (such as coupling between solid core fibers and microstructured fibers).

As such there is a need to thermally isolate or compensate fiber optic components. Manufacturers typically package these components so as to minimize this impact, employing bulky insulated enclosures, jacketing the fiber with insulating and/or reflecting layers [1], or utilizing complicated techniques and expensive materials. These techniques often employ negative CTE (coefficient of thermal expansion) materials or bimetals to athermalize the component. The materials used in the athermalization process are often exotic ([2], [3]), utilizing materials such as β-eucryptite [4] or extruded liquid crystal polymers [5]. Another technique involves intensive handling, whereby plies of carbon fiber strands are woven into a contrahelical or braided pattern [6]. Other approaches use bimetallic structures that must be perfectly matched to the host material to negate the CTE of the optical fiber [7], [8], [9], [10], [11], [12]. While effective at suppressing temperature fluctuations, these approaches are not easily realized by the average end user. Furthermore, these compensation materials are often only available on pre-packaged components not accessible for aftermarket or in-house fabricated optical devices.

To minimize thermal fluctuations from affecting fiber optic components, passive temperature control via insulation can be used. To insulate the grating from the environment, a novel packaging technique utilizing an evacuated air gap between welded glass capillaries in a concentric configuration has been devised. The design of the fiber optic thermal insulator (FOTI) uses a double wall structure reminiscent of those found in cryogenic liquid storage vessels [13], vacuum insulated pipes [14] or panels [15], or solar heat pipes [16]. In this design, the ends of the cylinders are sealed together leaving a central access port through the interior of the inner cylinder for fiber optic components. Once the fiber optic device is fed through the insulator, the evacuated gap eliminates the dominant radial conduction path to the component and reduces convection in the interstitial space. The addition of a thermal mass surrounding the optical component can also be utilized to increase the effective time constant of the fiber.

Manuscript approved February 25, 2019.

2. FABRICATION

In the present implementation, two different glass materials are used for the capillaries, fused silica and borosilicate glass. The fused silica tube served as the inner cylinder while the outer cylinder was comprised of borosilicate glass. The reason for this is the difference in the melting point between the two materials. Fused silica melts around 1600 °C while borosilicate softens at 800 °C. Thus, the borosilicate tube can be melted onto the fused silica tube, imparting no deformation to the inner tube. Note that careful control of the heat zone could permit use of a single type of glass, thereby minimizing thermally-induced stresses at the weld seams due to differences in CTEs between materials comprising the inner and outer cylinders.

To achieve concentricity between the two tubes, each tube can be independently clamped and aligned along a common longitudinal axis. Concentricity is achieved when the inner tube is able to cleanly pass through the outer tube and has equal margins of interstitial space in the transverse directions. Another approach would be to create an alignment jig that allows the ends of the tubes to be placed in such a manner that they are forced into concentricity. An appropriate design would act as end caps with protruding rings on which the capillaries would fit. The assembled tubes could then be clamped and processed.

The outer tube is sealed to the inner tube using a suitable heat source. Heat sources that provide a uniform distribution of heat around the capillaries are preferred as they ensure an even and symmetric weld. Examples might include large area isothermic plasma fields and filament heating elements typically employed in fiber optic glass processing machines, multiple burner micro-torches, or annular heating by a CO_2 laser beam. Fabricating the insulator vertically would also be advantageous. This geometry allows the melted glass to flow symmetrically about the inner tube, rather than slumping to one side due to gravity. Mounting the tubes horizontally in a rotating lathe would also produce a uniform weld. Sealing one end of the outer tubes allows a vacuum to be pulled on the structure, after which, the other end can be sealed creating an evacuated region between the two tubes. The remaining glass structure can then be cleaved or polished down beyond the sealed ends.

To protect the thermal insulator, the tubes can be placed inside a metal or other rigid cylinder and potted with an appropriate encapsulant. The assembled piece can then be thread onto the fiber optic component and fixed using a suitable adhesive. A v-groove assembly block can be utilized to ensure coaxially placement of the fiber within the insulator. Note the fiber component should have minimal tension to prevent temperature-induced elongation of the insulator from staining the fiber. Additional low thermal conductivity fillers, such as aerogel granules or powders, could be employed within the central region to limit motion of the fiber and further insulate the component.

2.1 Isothermic Plasma Field

To test the proof of concept, a prototype insulator was fabricated using a commercial glass processing station capable of producing an isothermic plasma field (3SAE LDS II). The borosilicate tube had an inner diameter (ID) of 1.6 mm and an outer diameter (OD) of 1.8 mm. The fused silica tube had an ID of 550 μm and an OD of 1.1 mm. The overall length of the capillaries was approximately 50 mm. Concentricity was achieved by loading both tubes in a single clamp and using a spacer to force concentricity. To prevent the glass from overheating, the plasma field was scanned rapidly over the tubes to limit their time in the hot zone. Additionally, the electrodes in the LDS were ramped from low to high power while the tubes were inserted into the plasma field (Fig. 1). Placement of the tubes within the plasma field was critical as the plasma field was deflected by the capillaries. The entire process was generally completed within 30 seconds.

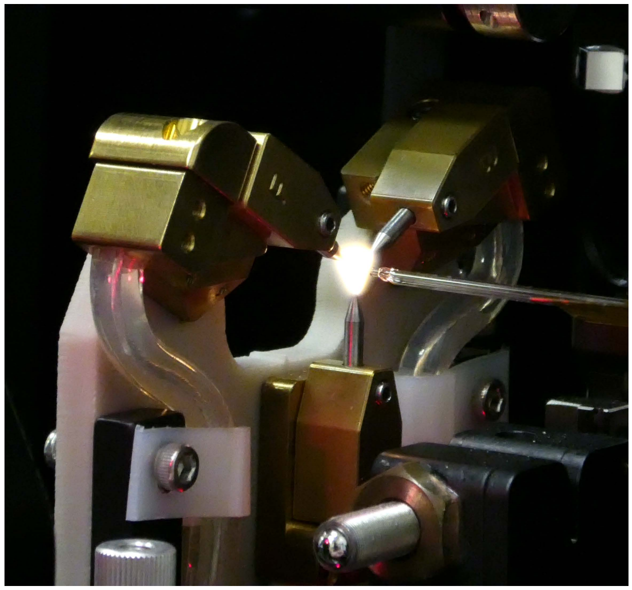

Fig. 1 — Insertion of capillaries into the plasma field of a 3SAE LDS II glass processing station.

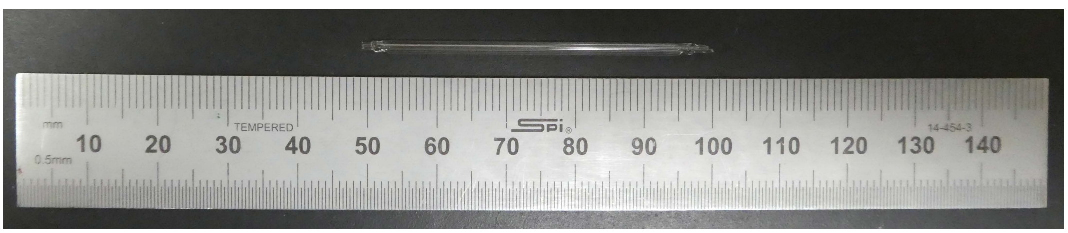

Fig. 2 — Welded thermal insulator comprised of borosilicate and fused silica capillaries fabricated via an isothermic plasma field.

The insulator was then flipped, and the other side was processed in a similar fashion. The finished insulator is shown in Fig. 2.

After fabrication, fiber Bragg gratings (FBGs) were used to measure the temperature response of the insulators. The FBGs were 25 mm long uniform gratings written in Corning's SMF-28 optical fiber. To prepare the samples, the FBGs were first recoated then thread through the insulators under minimal tension. Afterwards. they were potted to the ends of the tubes with Norland optical adhesive #68.

2.2 Isobutane Micro-Torch

Another set of insulators were fabricated using an isobutane micro-torch as the heat source. Here, three different sizes of capillary tubes were employed. The outer tube was made of borosilicate glass, had an OD of 2.4 mm and an ID of 2.0 mm, and was cleaved to 75 mm. The inner tube was fused silica, had an OD of 1 mm and an ID 0.8 mm, and was cleaved to 90 mm. This created a 0.5 mm annulus around the central tube. To help the capillaries remain concentric, an 80 mm spacer capillary tube made of fused silica was used. It had an OD of 1.65 mm and an ID of 1.15 mm (though ideally, the OD would be closer to 2.0 mm to further improve the concentricity of the inner tube). Next, the fused silica tubes were inserted into the borosilicate tube. The inner tube was pushed just past the end of the borosilicate tube and secured with Kapton tape to prevent movement during the collapse. The isobutane torch was then used to melt the borosilicate tube around the silica inner tube (Fig. 3). The tubes were rotated and translated in and out of the flame by hand during the collapse to minimize rapid melting of the borosilicate tube.

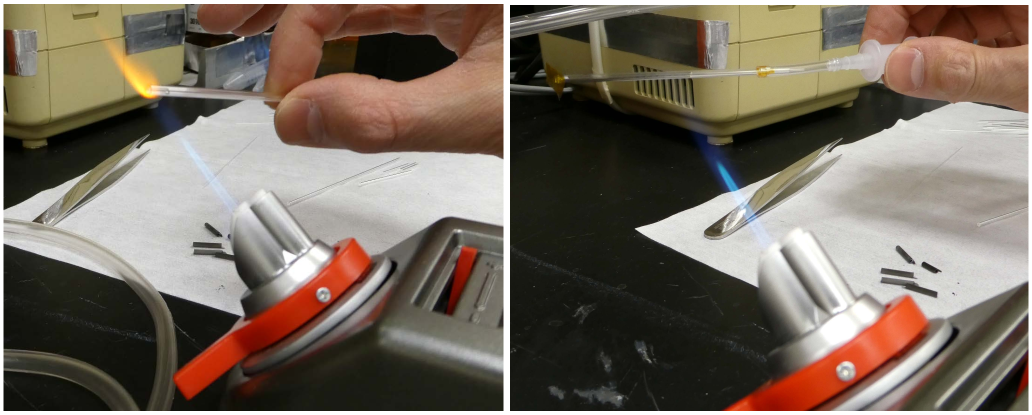

Fig. 3 — Initial (Left) and final (Right) collapse of the capillary tubes using an isobutane micro-torch.

Next, the spacer tube was removed and new spacer about 40 mm in length was inserted into the capillaries. This established a 45 mm region of insulation. A small piece of Kapton tape was used to secure the tubes together. A mini-pump vacuum (Linicon LV-125A) was then used to evacuate the interstitial space. Though incapable of achieving sufficient vacuum (330 mbar versus 1×10^{-3} mbar needed to achieve ideal insulation), it provided a means to test the approach. A small length of tubing connected the proximal end of FOTI (the uncollapsed portion) to the vacuum pump. The distal end of the FOTI was "capped" with a piece of Kapton tape so that a vacuum could be pulled. Collapse of the tube then proceeded similarly as before (Fig. 3). Once completed, excess borosilicate capillary was cleaved from the FOTI. Figure 4 shows the finished FOTI after the final collapse and prior to cleaving. After fabrication, FBGs were then thread through the FOTIs and potted as before.

Fig. 4 — Welded thermal insulator comprised of borosilicate and fused silica capillaries fabricated via an isobutane micro-torch.

2.3 Stainless Steel Compression Housing

A final thermal insulator was fashioned using a 0.25 inch stainless steel compression union tee to provide a highly evacuated sample for comparison. Two 0.25 inch stainless steel tubes were used to extend the length

(18 mm on each side) of the fitting. The tubes were secured to the union tee, and the fiber was then thread through the openings. The tee was mounted vertically and the side port was used to visualize the fiber and grating location. The fiber was suspended such that it was nominally coaxial with the tube opening. Then, Torr Seal low vapor pressure epoxy was used to seal the end. Once one end had cured, the tee was rotated 180°, and the other opening was sealed in the same manner. The completed specimen is illustrated in Fig. 5. Afterwards, the union tee was connected to a Pfeiffer vacuum (model TSH0701E) and pumped to a pressure below 5×10^{-6} mbar.

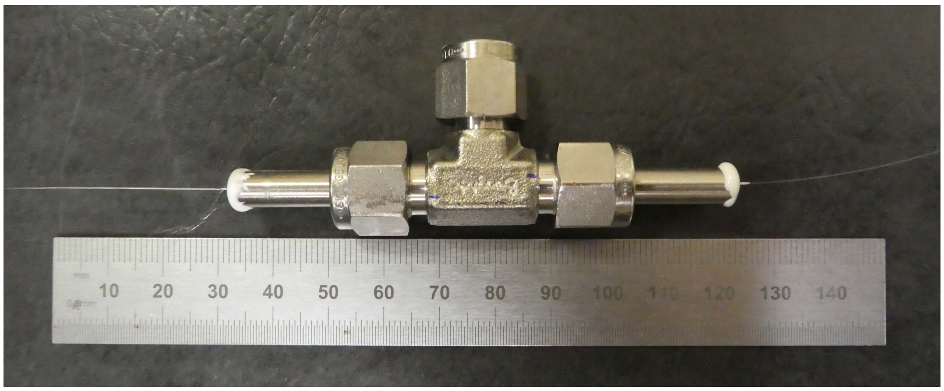

Fig. 5 — Epoxied thermal insulator utilizing compression fittings with a port for evacuating the inner chamber.

3. EXPERIMENTAL SETUP

To determine the effectiveness of the thermal insulators, the thermal time constant for each device was measured several times and averaged. This involved subjecting the insulators to a sudden change in temperature and monitoring the wavelength shift of the FBGs. The thermal time constant is defined as the time it takes for the component to reach 63.2% (i.e. $1-1/e$) of a step change in temperature and is dependent on the heat transfer between the outside environment and the fiber core. The temperature step was facilitated using a shallow thermal bath made by Polyscience (Fig. 6). The heat transfer fluid was PDM-1922 silicone thermal fluid by Gelest, and the temperature set point was varied between 25 °C and 100 °C.

The bath and ambient temperature were monitored using National Instruments USB-TC01 thermocouple readers. A u-shaped mount attached to a standard 0.5 inch optical post positioned the insulators inside the oil bath (Fig. 6). The ends of the FOTIs were attached with Kapton tape so that the central portion could be immersed in the liquid. Prior to insertion, the u-mount was moved just above the post holder (shown to the right of the bath in Fig. 6) for 10 to 20 seconds for a baseline measurement. A locking collar fixed to the mounting post was used to consistently locate the u-mount into the post holder and set so that the depth of insertion was approximately 45 mm from the bottom of the chamber. The FOTI was then plunged into the silicone fluid at a rate approximately 5 cm/s. The FOTI stayed in the bath for approximately 10 mins, after which it was removed, dunked into a clean water bath, and rinsed with isopropyl alcohol.

To test the evacuated FOTI, the insulator was connected to the turbopump using a flexible metal hose. A high temperature heat gun was used to bake the vacuum line and any fittings where volatiles might be present. An ion gauge and a Pirani gauge were installed to monitor the low and high pressure, respectively,

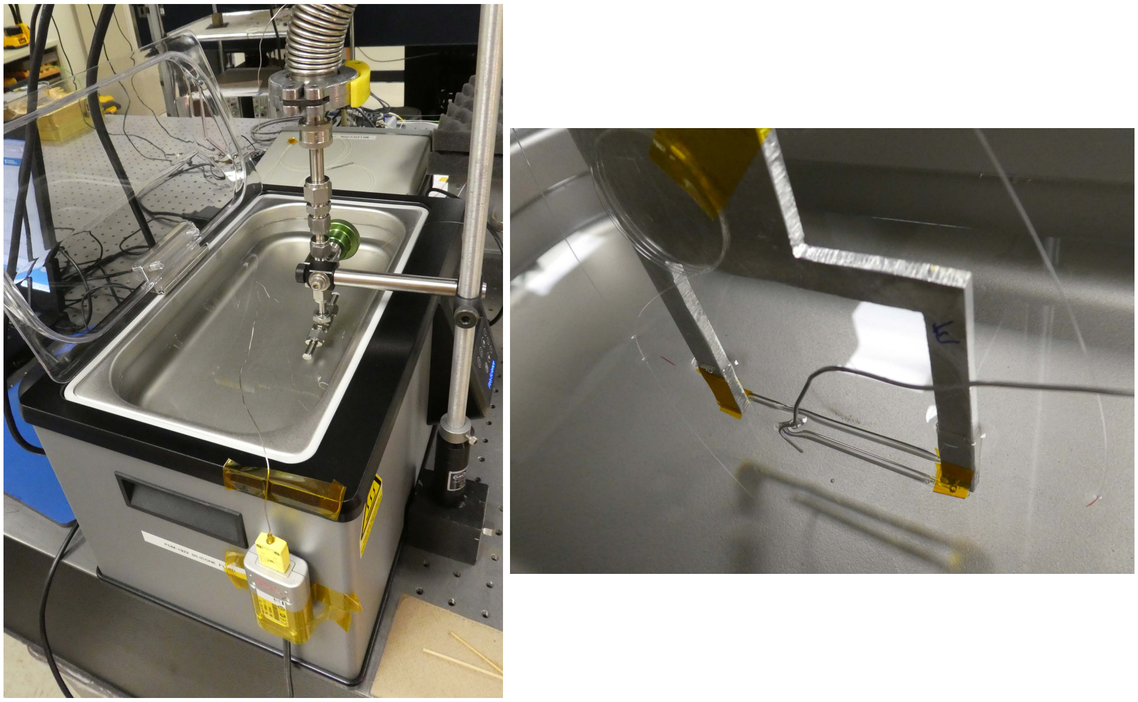

Fig. 6 — (Left) Temperature bath setup for measuring the thermal response of FOTIs. The evacuated insulator is shown mounted. (Right) U-shaped fixture used to mount the capillary FOTIs for testing in the oil bath. A K-type thermocouple probes the oil temperature at the insertion depth.

and an SRS IGC100 ion gauge controller was used to read the meters. Quick connect fittings were primarily used except for the connections to the pressure gauges. A purge line was also added to facilitate backfilling of the fiber insulator with dry nitrogen gas. During most experiments, the valve connecting the insulator to the vacuum was set open to allow continuous pumping. This prevented any atmosphere from entering the housing should a leak occur. Vibration and acoustic noise were minimal and did not interfere with the experiment. Insertion of the FOTI into the temperature bath proceeded as described earlier. A picture of the submerged evacuated insulator is shown left in Fig. 6.

The wavelength shifts of the gratings under test were monitored using interferometric interrogation. A schematic of the setup is shown in Fig. 7. An erbium broadband source (BBS) was launched into a fiber optic Michelson interferometer with a 3.2 mm roundtrip optical fiber path imbalance. Faraday rotation mirrors (FRM) were utilized to reduce any birefringence in the fiber leads of the interferometer. One arm of the interferometer was driven with a sinusoidal phase generated carrier (PGC) using a piezoelectric transducer at 20 kHz. The output from the interferometer was then passed to a 1$\times$3 fiber coupler to simultaneously measure three test samples. A circulator (CIRC) was used to facilitate readout of the reflection spectrum. The light signal was then detected with TTI-525 low-noise InGaAs detectors. The signals were digitized using a National Instruments X-series USB DAQ board. A laptop controlled the acquisition of the data and demodulation of the signal [17]. The data was sampled at a rate of 300 kHz. Note that one channel (i.e. a reference grating) was always used to subtract common mode effects (such as environmental drift) from the interferometer.

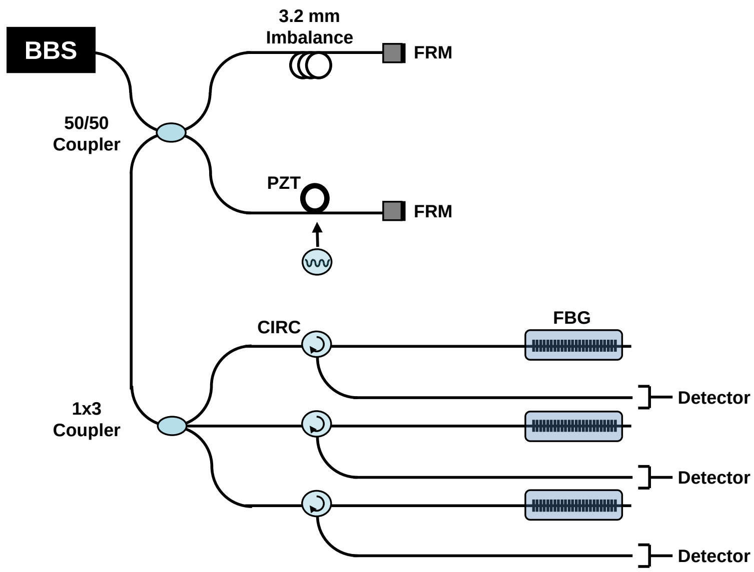

Fig. 7 — Demodulation system for FOTI test measurements. BBS = Broadband Source, FRM = Faraday Rotating Mirror, PZT = Piezoelectric Tube, CIRC = Circulator.

4. RESULTS

4.1 Thermal Time Response

The thermal response curves for the various FOTI designs are illustrated in Fig. 8. The average time constants for each design are reported in Table 1. Using a log scale, the relative time scales between each FOTI variant can easily be viewed. The bare fiber responded the quickest, followed by a single-walled capillary (simply an FBG potted within the 1.1 mm OD/0.55 mm ID fused silica tube), then the double-walled concentric capillaries, and finally the evacuated FOTI. The time constant of bare fiber was on the order of 40 ms. When the fiber was coated with a standard acrylate coating (250 μm OD), the time constant increased to 110 ms. Placing the fiber in the silica tube further increased the time constant to 1.8 s, and if concentric capillaries were employed, the time constant stretched to 5 s. The stainless steel insulator under two conditions, atmospheric pressure and vacuum, had time constants of 152 s and 197 s, respectively. By creating an evacuated sample, the time constant increased from 40 ms to 200 s, a factor of 5000 improvement. While not in the spirit of the original design, the evacuated FOTI demonstrated the highest performance implementation of the device possible. The doubled-walled insulator showed 125 times improvement over bare fiber and almost a factor of 3 improvement over the single-walled insulator. Evacuating the interstitial space and further minimizing the conduction paths should improve the double-walled insulator's performance. Physical modeling of the FOTI using COMSOL is needed to determine the optimum parameters (such as capillary dimensions) and resulting performance.

Of note in Fig. 8 are the curious wiggles seen at the top of the response curves. Although instrumentation errors cannot be ruled out, another possible explanation for this behavior is the acrylate coating on the fiber. Ideally, the bare fiber should be directly adhered to the insulator to decouple the coating from the capillaries. Unfortunately, the fiber coating was not stripped when the gratings were potted inside the FOTIs. As a result, expansion of the coating in the oil bath (caused by its CTE) could potentially transfer some strain down the

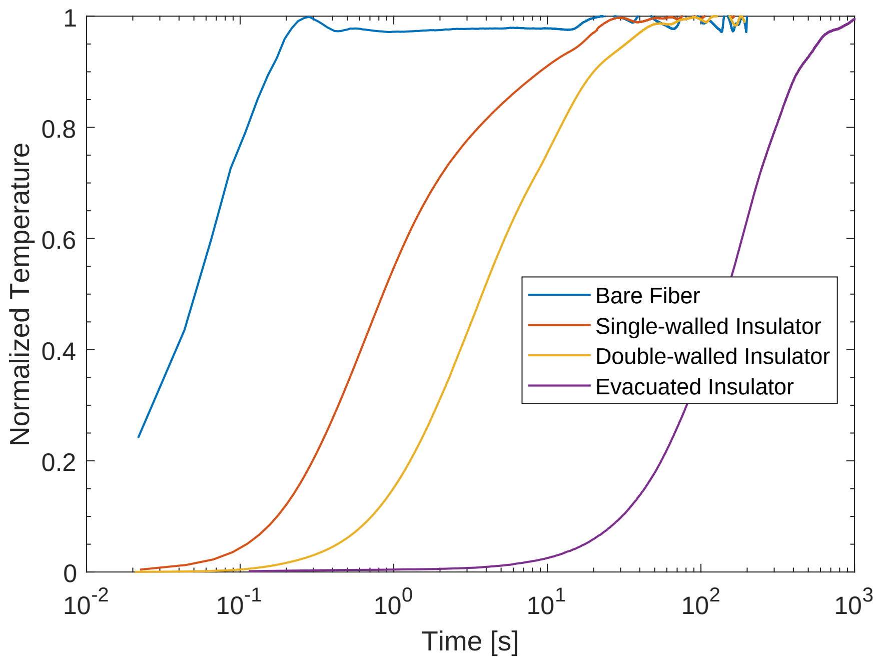

Fig. 8 — Temporal response for various insulator designs. The temperature has been normalized here to account for slight differences in experimental parameters (temperature differentials ranged from 16 °C to 18 °C).

fiber and affect the FBG since the epoxy seals around the fiber coating instead of the glass. Because the thermal insulator responds at a rate independent of the coating, the competing effects of these two processes coming to equilibrium could partly explain the undulations.

Table 1 — Temporal Responses of various FOTI designs

FOTI	Time Constant [s]	Error [±s]
Bare Fiber	0.043	0.01
Jacketed Fiber	0.11	0.02
Single-walled Insulator	1.80	0.40
Double-walled Insulator	5.00	0.92
Evacuated Insulator (air)	151.67	12.87
Evacuated Insulator (vacuum)	197.36	12.2

The performance of the FOTIs were also characterized by monitoring the reported temperature fluctuations in an open lab environment. In this experiment, the bare fiber, double-walled insulator, and evacuated FOTI were collocated in space and simultaneously sampled. A K-type thermocouple was also placed in close proximity to record the ambient temperature fluctuations. Figure 9 illustrates the excellent thermal resistance of the various insulating devices. The thermocouple data is also plotted (in black), showing that the gratings correctly report the temperature in the lab (acquired at 1 sample/s). Clearly the evacuated FOTI demonstrates the greatest thermal resistance, showing little variation over the 200 s window displayed here.

The double-walled insulator also shows a marked improvement over the bare fiber. Fluctuations, as represented by the variation in temperature over a short time window, span 2.72 °C, 1.16 °C, and 0.08 °C for the bare fiber, double-walled insulator, and evacuated fiber, respectively. If we assume the temperature response of the gratings to be 14 pm/°C, then the temperature swings will result in wavelength errors of 38 pm, 16 pm (or 6 pm/°C), and 1 pm (0.4 pm/°C) for the bare fiber, double-walled insulator, and evacuated FOTI, respectively.

The plot to the right in Fig. 9 shows the power spectral density of the temperature variations depicted in the left figure. From this graph, the filtering effect of each FOTI can be seen. The improvement gained by insulating the gratings is apparent. At a frequency of 1 Hz, both the double-walled and evacuated FOTIs provide almost 30 dB of suppression. Below 1 Hz, the evacuated FOTI maintains 30 dB of suppression until 0.04 Hz. The double-walled insulator also provides improved performance over the bare fiber, but diminishes with decreasing frequency. At higher frequencies, the effect of insulating the grating decreases as even for bare fibers, the heat does not have enough time to conduct through the cladding to the core.

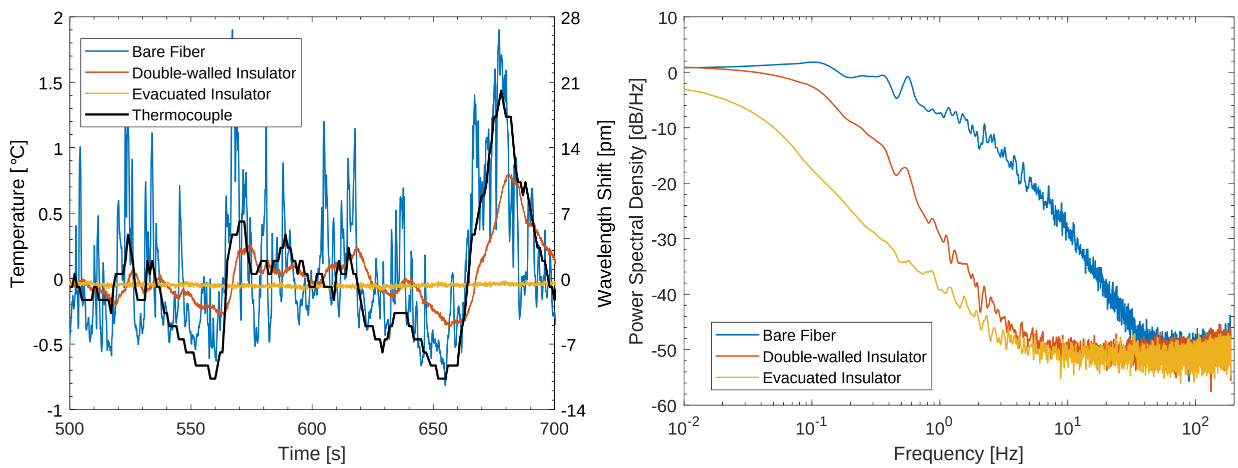

Fig. 9 — (Left) Temperature fluctuations as experienced by various insulator designs and a K-type thermocouple. (Right) Power spectral density of the temperature data to the left.

4.2 Time Constant Dependence on Temperature

In another series of experiments, the evacuated FOTI was characterized over a range of temperature differentials. This was also repeated with the insulator at atmospheric pressure. As seen in Fig. 10, the time constant depends on the difference between the temperature of the oil bath and air above the basin. For the FOTI in air, the time constants range from 100 s to 150 s. In vacuum, the time constants span from 130 s to 190 s. Under both conditions, the time constant decreases with increasing temperature differential. A linear fit shows a slope and intercept of ~ 0.8 s/°C and 152 s, respectively, under atmospheric conditions and ~ 0.9 s/°C and 199 s, respectively, when evacuated. There is also a noticeable amount of scatter in the data shown in the plots. This is likely due to slight differences in the experimental conditions between measurements and the subsequent processing of the data. These variations might include convective heating from the oil bath warming the insulator or a misreporting of the actual temperature of the FOTI prior to insertion (i.e. the grating is not at the same temperature as ambient).

The observed dependence of the time constant on the temperature delta is possibly due to expansion of the metal housing and to a lesser extent, swelling and elongation of the fiber coating. Since the fiber was potted under some nominal tension during fabrication, any expansion of the housing will strain the fiber and cause the grating to experience tension. If the rate of expansion is faster than conduction through the fiber (and air within the FOTI if applicable), then the resultant thermal response curve could be explained as a combination of these two processes. Because stainless steel has a higher thermal conductivity than the fiber (13 W/m·K vs 1.4 W/m·K), the housing heats up faster than the fiber and approaches its equilibrium state first. And since the expansion is proportional to the temperature, a larger response would be expected for higher temperature differentials. This same scenario also applies when the FOTI is at atmospheric pressure, but in this case, conduction can also occur through the air molecules within the insulator. Future implementations of the FOTI should ensure that the grating is relaxed to prevent thermal expansion of the housing from straining the fiber. Were the grating strain-relieved within the housing, it is likely that the time constants under both conditions would be close to the intercept values referenced above regardless of the temperature differential, demonstrating more than a 30% improvement in the insulating capability through evacuation.

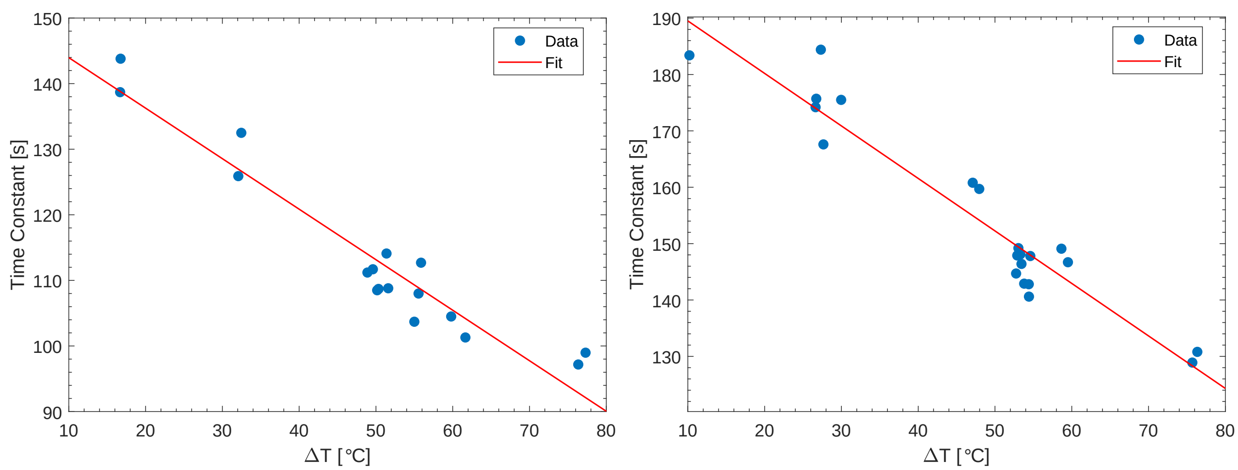

Fig. 10 — (Left) Time constant of the evacuated FOTI (at atmospheric pressure) for different temperature differentials. (Right) Time constant of the evacuated FOTI (in vacuum) for different temperature differentials.

4.3 Time Constant Dependence on Pressure

In this experiment, the evacuated FOTI was backfilled with nitrogen to investigate the dependence of the time constant on vacuum pressure. The pressure was monitored using the ion and Pirani gauges at the proximal end of the flexible hose. Each measurement consisted of bleeding nitrogen into the system to a fixed pressure, closing the valve, then submerging the FOTI into the oil bath at a 55 °C temperature differential. The temperature response was then recorded and the time constant calculated. This process was repeated until the FOTI was at atmospheric pressure. The left plot of Fig. 11 shows the data taken at various pressures and their resulting thermal response. As the pressure in the housing decreases, the time constant increases, delaying the transfer of heat to the grating. The data can be fit to a logistic function of the form

$$\tau(p) = a + \frac{b-a}{1+cp}, \tag{1}$$

where $\tau(p)$ is the time constant as a function of pressure p, and a = 107.93, b = 146.71, and c 192.65 are the fit coefficients. The three variables represent the saturation values (a, b) and the steepness of the curve (c). The data illustrates that there is roughly a 36% improvement by evacuating the chamber. It also shows that reducing the pressure beyond 1 $\times 10^{-3}$ mbar does little to improve the insulating properties.

The pressure response can be understood by examining the thermal conductivity of air as a function of pressure. The thermal conductivity of air, κ_{air}, between two plates within an enclosed cavity can be estimated as [18]

$$\kappa_{air}\left[\frac{W}{mK}\right] = \frac{\kappa_0}{1+\frac{7.6\times10^{-5}}{\frac{pD}{T_{avg}}}}. \tag{2}$$

Here, κ_0 represents the thermal conductivity at atmospheric pressure, D is the distance between plates, and T_{avg} is the average temperature. The factor 7.6 $\times 10^{-5}$ is a coefficient that depends on the gas properties. The plot to the right in Fig. 11 shows the thermal conductivity for various plate separations. Most notable is that there is little difference in the thermal conductivity below a pressure of 1 $\times 10^{-3}$ mbar, aligning well with the measured data to the left.

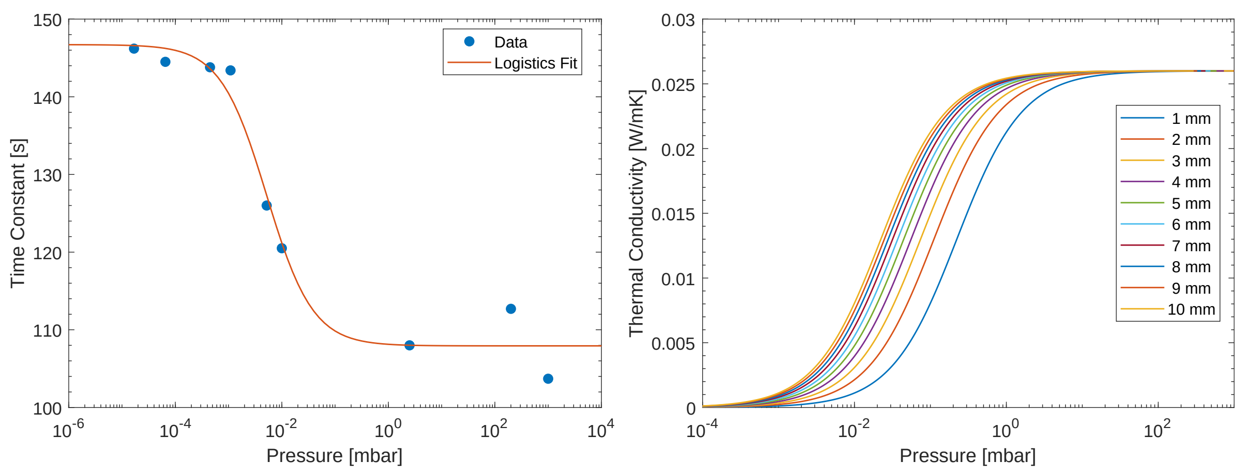

Fig. 11 — (Left) Time constant for the evacuated FOTI as a function vacuum pressure. (Right) Thermal conductivity of air between two plates in an enclosed chamber as a function of vacuum pressure and plate separation.

5. CONCLUSIONS

The utilization of a passive insulator in place of various athermalization or insulation techniques has several advantages. For many applications, a fiber optic device will only be operated within a narrow temperature range, thus temperature compensation over a wide range is not needed. In these instances, a passive insulator of the present design can minimize temperature fluctuations sufficiently when compared to athermalization techniques. Since an evacuated gap provides superior thermal isolation, the device also greatly improves over insulation designs where the fiber is simply sheathed in foam or other insulating materials. In the present design, the amount of thermal suppression (i.e. the temporal response) can easily be adjusted by controlling level of vacuum pulled on the interstitial space between tubes. A device of this design can also achieve satisfactory performance in packages on the order of a few millimeters in diameter. Perhaps the most significant advantage of this invention is the ability to utilize an insulator of this type with aftermarket or in-house fabricated fiber optic devices. No commercial product currently exists that can be oversleeved on an optical fiber and provide a similar level of insulation, upwards of 30 dB improvement in limiting temperature fluctuations with a time constant 5000 times greater than bare fiber.

ACKNOWLEDGMENTS

Funding for this project was provided by internal NRL base funding.

REFERENCES

1. H. Davidson, “Low thermal skew fiber optic cable,” *US Patent* **6028975** (February 2000).
2. D. Fleming, D. Johnson, and P. Lemaire, “Article comprising a temperature compensated optical fiber refractive index grating,” *US Patent* **5694503** (Dec 1997).
3. J. Albert, “Adjustable temperature compensating package for optical fiber devices,” *US Patent* **6807341** (October 2004).
4. G. Beall, K. Chyung, and J. Pierson, “Athermal optical device,” *US Patent* **6087280** (July 2000).
5. T. Wakami, M. Shigematsu, Y. Terasawa, A. Inoue, M. Shigehara, and T. Iwashima, “Optical fiber diffraction grating, a method of fabricating thereof and a laser light source,” *US Patent* **6067392** (May 2000).
6. P. Ogle, “Optical fiber having a bragg grating in a wrap that resists temperature-induced changes in length,” *US Patent* **6466716** (October 2002).
7. C. Miller, “Temperature compensated fiber bragg gratings,” *US Patent* **6044189** (March 2000).
8. J. Engelberth, R. Espindola, S. Jin, P. Lemaire, and H. Mavoori, “Temperature-compensated optical fiber bragg gratings with fine wavelength tuning,” *US Patent* **6101301** (August 2000).
9. R. Enochs and R. Randall, “Temperature-compliant tube for fiber optic components,” *US Patent* **4936646** (June 1990).
10. I. Lin, “Temperature-compensating device with tunable mechanism for optical fiber gratings,” *US Patent* **6374015** (April 2002).
11. J. Bulman and H. Inglis, “Temperature stable bragg grating package with post tuning for accurate setting of centre frequency,” *US Patent* **6393181** (May 2002).
12. R. Lachance, A. Van, M. Morin, M. Guy, and M. Pelletier, “Adjustable athermal package for optical fiber devices,” *US Patent* **6907164** (June 2005).
13. R. Burger, “Double-walled vessel with a space for a vacuum between the walls,” *US Patent* **872795** (December 1907).

14. C. Trucano, "Insulating system," *US Patent* **1140633** (May 1915).

15. D. Comstock, "Building construction," *US Patent* **1770200** (July 1930).

16. F. Fehlner and U. Ortabasi, "Solar heat pipe," *US Patent* **4067315** (January 1978).

17. A. Dandridge, A. Tveten, and T. Giallorenzi, "Homodyne demodulation scheme for fiber optic sensors using phase generated carrier," *IEEE Journal of Quantum Electronics* **18**(10), 1647–1653 (October 1982), doi: 10.1109/JQE.1982.1071416.

18. H. Wu, S. Grabarnik, A. Emadi, G. de Graaf, and R. F. Wolffenbuttel, "Characterization of thermal cross-talk in a mems-based thermopile detector array," *Journal of Micromechanics and Microengineering* **19**(7), 074022 (2009).